Relativistic laser hosing instability suppression and electron acceleration in a preformed plasma channel

T. W. Huang,[1] C. T. Zhou,[1,2,3,4,*] H. Zhang,[4] S. Z. Wu,[4] B. Qiao,[3] X. T. He,[3,4] and S. C. Ruan[1,2,†]

[1]*College of Optoelectronic Engineering, Shenzhen University, Shenzhen 518060, People's Republic of China*

[2]*College of New Energy and New Materials, Shenzhen Technology University, Shenzhen 518118, People's Republic of China*

[3]*HEDPS, Center for Applied Physics and Technology, School of Physics, Peking University, Beijing 100871, People's Republic of China*

[4]*Institute of Applied Physics and Computational Mathematics, Beijing 100094, People's Republic of China*

(Received 2 November 2016; revised manuscript received 16 March 2017; published 17 April 2017)

The hosing processes of a relativistic laser pulse, electron acceleration, and betatron radiation in a parabolic plasma channel are investigated in the direct laser acceleration regime. It is shown that the laser hosing instability would result in the generation of a randomly directed off-axis electron beam and radiation source with a large divergence angle. While employing a preformed parabolic plasma channel, the restoring force provided by the plasma channel would correct the perturbed laser wave front and thus suppress the hosing instability. As a result, the accelerated electron beam and the emitted photons are well guided and concentrated along the channel axis. The employment of a proper plasma density channel can stably guide the relativistically intense laser pulse and greatly improve the properties of the electron beam and radiation source. This scheme is of great interest for the generation of high quality electron beams and radiation sources.

DOI: 10.1103/PhysRevE.95.043207

I. INTRODUCTION

With the rapid development of laser technology, laser based plasma accelerators and radiation sources have become an important complement to the conventional ones [1]. Particularly, in the interaction of a relativistic laser pulse with the underdense plasmas, electrons can be accelerated to highly relativistic energy [2–8], and high brightness synchrotron x rays can also be produced through the betatron oscillations [9–12]. Depending on different laser and plasma parameters, the laser driven electron acceleration can roughly be divided into two regimes. One is the laser wakefield acceleration (LWFA) in which the electron gains its energy from the longitudinal charge separation electric field [13]. The other regime is the direct laser acceleration (DLA) in which the electron gains its energy directly from the transverse laser field [14]. In the LWFA regime, the electron dephasing process determines that a high-energy electron beam always corresponds to a low-charge number [15]. Whereas in the DLA regime of an ultraintense laser pulse interacting with the near-critical density plasmas, electron beams with both high energy and high charge are produced easily [16–20]. In addition, it was suggested that high-energy and high-flux radiation sources can also be achieved by exploiting this regime [21,22]. However, in this regime, when the relativistic laser pulse propagates into the near-critical plasmas, it will suffer from many instabilities, such as the filamentation instability and hosing instability [23–34]. These nonlinear processes will make the generated electron beam and radiation source uncontrollable. Understanding how to suppress these nonlinear processes is a critical issue as it underpins the development of laser based plasma accelerators and radiation sources.

To suppress and control the filamentation process, several methods have been proposed in our earlier works. It was proposed that the filamentation process can be manipulated by employing an elliptically distributed laser beam [35] or the optical vortex beams [36]. Particularly, in a self-matched propagation condition, the filamentation instability would not occur [37]. However, for a relatively long time propagation behavior, the laser hosing instability, which is triggered by the transverse asymmetric laser intensity or plasma density perturbations, would grow up inevitably [28]. This kind of instability leads to the titling of the laser propagation direction, which in turn leads to the generation of uncontrollable and mistargeted electron beams. Thereby, the laser hosing process severely limits the usefulness of laser based plasma accelerators and radiation sources. In previous studies, specially engineered targets [38–44], such as the capillary tube target, cone target, the sandwiched target, and the plasma density channel, have been employed to guide the laser pulse and thus the electron beam in plasmas. Here, especially in the DLA regime, the dependency of hosing instability on different plasma density profiles and the caused effects on electron dynamics and radiation properties are explored.

In this paper, the underlying dependency of laser hosing instability on different plasma density profiles is investigated. The corresponding electron dynamics and radiation properties also are explored in the DLA regime. It is proposed that a parabolic plasma channel with a radially symmetric density profile that has a minimum on its central axis can be used to suppress the laser hosing instability. The laser hosing process leads to the generation of uncontrollable off-axis electron beams and radiation sources. While in a preformed parabolic plasma channel, electrons can be well guided along the channel axis, and the emitted photons are directed with a smaller divergence angle compared with the case without a preformed plasma channel. The paper is organized as follows. In Sec. II, theoretical analyses on the laser hosing instability in a preformed plasma channel are given. In Sec. III, particle-in-cell simulations are conducted to verify the theoretical predications on hosing instability. The corresponding electron dynamics and radiation properties also are investigated. The conclusion is given in the final section.

*zcangtao@iapcm.ac.cn

†scruan@szu.edu.cn

II. THEORETICAL ANALYSES

When a relativistic laser pulse propagates into the plasma, its propagation direction will undergo transverse tilt due to the hosing instability, which is induced by the transverse asymmetric perturbations. These asymmetries can result from the beam noise and the perturbations of the plasma density. The asymmetric perturbations lead to the asymmetric distribution of the laser phase velocity, which is dependent on the laser intensity and the plasma density. Then the pulse wave front and its propagation direction will be tilted. This is the physical picture of the hosing instability that was proposed by Ren and Mori [28]. It is noted that previous theoretical studies on hosing instability are mainly based on a weak relativistic limit and low plasma density assumption [28–31]. Recently, a new physical model that incorporates the relativistic effect and moderate plasma densities was presented, and it was indicated that the laser hosing instability is reduced due to the relativistic effect, which can increase the relativistic critical density and thus reduce the effect of density perturbations on the laser phase velocity [32]. Here we are concerned with the hosing instability of an intense laser pulse in a preformed plasma channel with different density profiles in the ultrarelativistic regime.

To begin, a slab geometry is considered. An ultraintense laser pulse with $a \gg 1$ is assumed to propagate along the x direction and polarize in the y direction. Here a refers to the normalized amplitude of the laser field. The initial density profile of the plasma channel is assumed as $n_{e0} = n_0(1 + \alpha y^2/L^2)$, where n_0 refers to the plasma density along the channel axis, α describes the steepness of the plasma channel, and L denotes the transverse size of the plasma channel. The phase velocity of the ultraintense laser pulse propagating in the plasma can be written as $v_{\rm ph} = c/\sqrt{1-\omega_p^2/\omega_L^2} = c/\sqrt{1-n_e/\gamma n_c}$ [45], where ω_p is the plasma frequency, ω_L is the laser frequency, $\gamma = \sqrt{1+a^2/2}$ is the averaged Lorentz factor, and n_c is the critical plasma density. Assuming an asymmetric perturbation on the plasma density, i.e., $n_e = n_{e0} + n_{e1}$, then the phase velocity can be expanded as

$$\frac{v_{\rm ph}}{c} \approx \sqrt{\frac{\gamma n_c}{\gamma n_c - n_{e0}}}\left[1 + \frac{1}{2}\frac{n_{e0}}{\gamma n_c - n_{e0}}\frac{n_{e1}}{n_{e0}}\right]. \tag{1}$$

After some algebra, one can get the evolution equation for the centroid of the laser pulse (Y_c) [28,32],

$$\frac{\partial^2 Y_c}{\partial t^2} = -v_{\rm ph}\frac{\partial v_{\rm ph}}{\partial y}, \tag{2}$$

where Y_c is defined as $Y_c \equiv \int y E_y^2 d\vec{r} / \int E_y^2 d\vec{r}$ and E_y denotes the laser electric field. At the position near the laser centroid, by substituting Eq. (1) into Eq. (2), one has

$$\frac{\partial^2 Y_c}{\partial t^2} + \beta Y_c = -\frac{c^2}{2}\frac{\gamma n_c n_0}{(\gamma n_c - n_0)^2}\frac{\partial}{\partial y}\frac{n_{e1}}{n_0}, \tag{3}$$

where $\beta = \alpha\frac{c^2}{L^2}\frac{\gamma n_c n_0}{(\gamma n_c - n_0)^2}$. Here the second term in Eq. (3) is induced by the preformed plasma density profile, and the right-hand side of Eq. (3) represents the perturbation term for transverse tilting. It is noted that these expressions can be reduced into the form in previous works in a linear limit [30]. The density perturbation is induced by the laser ponderomotive force and can be described as

$$\left(\frac{\partial^2}{\partial \xi^2} + \frac{\omega_p^2}{c^2}\right)\frac{n_{e1}}{n_0} = \nabla^2\gamma, \tag{4}$$

where $\xi = v_g t - z$, $\nabla^2 = \frac{\partial^2}{\partial \xi^2} + \frac{\partial^2}{\partial y^2}$ is the Laplace operator, and v_g refers to the laser group velocity. In the weak relativistic limit, the right-hand side of Eq. (4) can be reduced as $\nabla^2\frac{a^2}{4}$, which is analogous to the previous expressions [28–31]. The corresponding solution of Eq. (4) can be written in an integral form as $\frac{n_{e1}}{n_0} = \int_{-\infty}^{\xi}\sin[\omega_p(\xi-\xi')/c]\nabla^2\gamma(\xi', y)d\xi'$. Particularly, in the so-called long wavelength regime ($\frac{\partial^2}{\partial \xi^2} \ll \omega_p^2/c^2$), Eq. (4) can be approximated as $\frac{n_{e1}}{n_0} = \frac{c^2}{\omega_p^2}(\frac{\partial^2}{\partial \xi^2} + \frac{\partial^2}{\partial y^2})\gamma(\xi, y)$. In an ultrarelativistic regime with $a \gg 1$, $\gamma \approx a/\sqrt{2}$. For the Gaussian laser beam with the profile of $a = a_0\exp(-y^2/R^2)$, the laser intensity can be expanded near the laser centroid as $a_0\{1 - [y - Y_c(\xi)]^2/R^2\}$, where R denotes the beam radius. Then one has

$$\frac{\partial}{\partial y}\frac{n_{e1}}{n_0} \approx \frac{\sqrt{2}c^2}{R^2\omega_L^2}\frac{a_0 n_c}{n_0}\frac{\partial^2 Y_c}{\partial \xi^2}. \tag{5}$$

Inserting this into Eq. (3) yields

$$\frac{1}{c^2}\frac{\partial^2 Y_c}{\partial t^2} + \beta' Y_c + \frac{c^2}{R^2\omega_L^2}\frac{1}{(1-\sqrt{2}n_0/a_0 n_c)^2}\frac{\partial^2 Y_c}{\partial \xi^2} = 0, \tag{6}$$

where $\beta' = \sqrt{2}\alpha\frac{1}{L^2}\frac{n_0/a_0 n_c}{(1-\sqrt{2}n_0/a_0 n_c)^2}$.

From Eq. (6) one can elucidate some characteristics of the hosing process for an ultraintense laser pulse in plasmas. It is shown that, for a plasma channel with $\alpha > 0$, the plasma density profile will provide an external restoring force on the laser centroid evolution. In this case, once the laser wave front is perturbed and tilted, the plasma density channel will introduce a transverse density asymmetry on the tilted laser pulse. For the tilted laser pulse in the plasma channel, its inner side closest to the channel axis will experience a lower plasma density than the outer side, leading to a phase velocity gradient with a lower phase velocity on the inner side than that on the outer side. Therefore, the plasma density profile will correct the titled wave front and thus reduce the hosing instability. On the contrary, for an antiplasma channel with $\alpha < 0$, once the laser pulse is tilted, its inner side will have a larger phase velocity than the outer side. Thus the repelling force provided by the antiplasma channel will further assist the development of the hosing instability. Thereby, the hosing instability depends strongly on the initial plasma density profiles. Particularly, it is possible to employ a preformed plasma density channel with a steep profile to suppress the laser hosing process. When the hosing instability is suppressed, the electron beam can be well guided along the channel axis and stably interact with the laser pulse. Meanwhile its emitted photons can also be directed along the channel axis. On the other hand, it can be seen from Eq. (6) that the hosing instability of the ultraintense laser pulse in plasmas only depends on a single self-similar parameter of $n_0/a_0 n_c$ [46]. The laser hosing instability becomes more severe for a larger parameter $n_0/a_0 n_c$, which can result from a larger plasma density or a lower laser intensity. In addition, the coefficient in the second term of Eq. (6), i.e., β', also is determined by a single parameter of $n_0/a_0 n_c$. Thus once

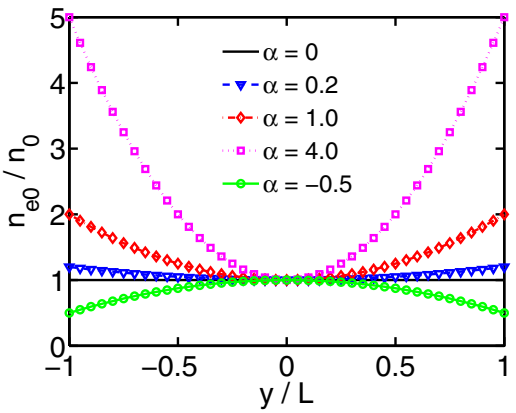

FIG. 1. The initial density profiles of different plasma channels.

the parameter $n_0/a_0 n_c$ and the value of α are fixed, the laser propagation processes in preformed plasma channels also become similar.

III. PARTICLE-IN-CELL SIMULATIONS

In the following, in order to confirm the above predications, two-dimensional particle-in-cell simulations were carried out using the EPOCH code, which can simultaneously calculate the laser propagation process, electron acceleration process, and the photon emission process [47]. In the simulations, a p-polarized Gaussian laser beam is irradiated into different plasma channels as shown in Fig. 1. The density profile of the plasma channel is defined as $n_{e0} = n_0(1 + \alpha y^2/L^2)$ where the channel size is set as $L = 12\lambda$ and the central laser wavelength is $\lambda = 1\ \mu$m. The laser has a flattopped temporal profile with a duration of $100T_L$, where $T_L = \lambda/c$ refers to the laser cycle and c is the light speed in vacuum. The simulation box is featured as $200\lambda \times 24\lambda$, and the grid size is set as $1/40\lambda$ along the propagation direction and $1/20\lambda$ on the transverse plane. Twenty-five particles of each species (electron and ion) are put in each cell. The mass ratio between the ion and the electron is set as 1836 in the simulations. The initial electron temperature is assumed to be 1 keV, and ion temperature is set as 10 eV. Here ultraintense laser pulses with $a_0 \geqslant 20$ and the near-critical plasma with the density $n_e \geqslant 1.2n_c$ are considered. In this case, the DLA regime plays a dominant role and leads to the generation of high-energy electron beams and radiation sources. In the simulations, different density profiles also are considered to investigate the hosing process, electron dynamics, and radiation properties. By exploiting the underlying dependence of these processes on the plasma density profiles, it would be of great interest for the development of laser based plasma accelerator and radiation sources.

A. The laser hosing process in different plasma channels

Figure 2 shows the simulation result for an ultraintense laser pulse with $a_0 = 60$ propagating through a uniformly distributed near-critical density plasma with $n_0 = 1.8n_c$ and $\alpha = 0$. The initial beam radius is set as 2.2 μm, which is about twice the relativistically corrected plasma skin depth ($2\sqrt{\gamma}c/\omega_p$). In this case, if the filamentation instability would not occur, then one can only focus on the hosing instability [22,35]. Here the moving window technique is not employed, but the simulation box is zoomed in, and the evolution process of the laser pulse is tracked as shown in Fig. 2. It is shown from Fig. 2(a) that, at the earlier stage, the laser beam can stably propagate in the plasmas and no filamentation instability is observed. In this case, a regularly microbunched electron beam is distributed in the central region as shown in Fig. 2(g). This is a typical characteristic of the direct-laser accelerated electrons [14,16–22]. The high-energy electrons would be confined by the channel field and experience transverse betatron oscillations in the plasma channel. In this process, high-energy and high-flux photons

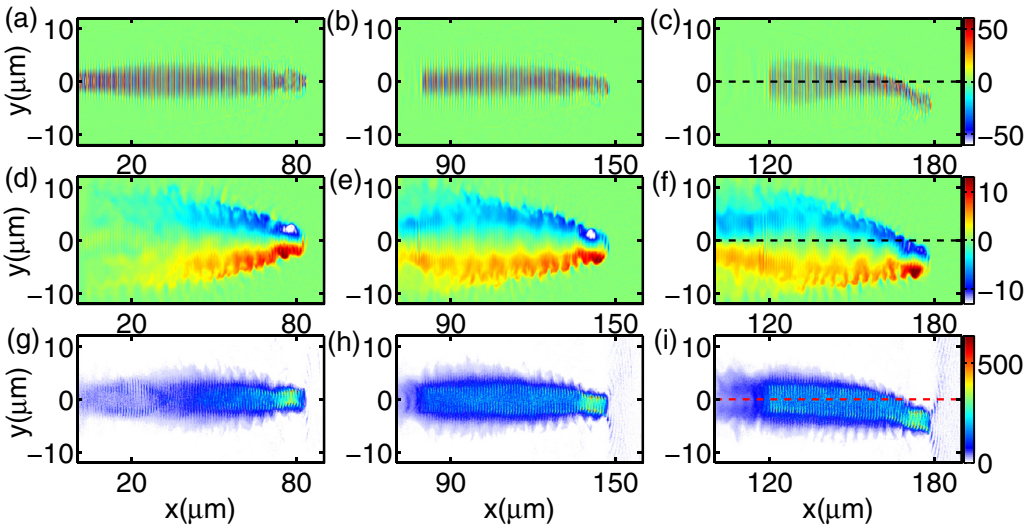

FIG. 2. The 2D particle-in-cell simulation results for $\alpha = 0$, $a_0 = 60$, and $n_0 = 1.8n_c$ at $T = 100T_L$ [(a), (d), and (g)], $T = 180T_L$ [(b), (e), and (h)], and $T = 220T_L$ [(c), (f), and (i)], respectively. (a)–(c) The distribution of the normalized transverse laser field ($eE_y/m_e\omega_0 c$) at three different times. (d)–(f) The corresponding transverse static magnetic field ($eB_{Sz}/m_e\omega_0$). (g)–(i) The distribution of the averaged electron energy (E_e) on the grids. The electron energy is in units of megaelectron volts.

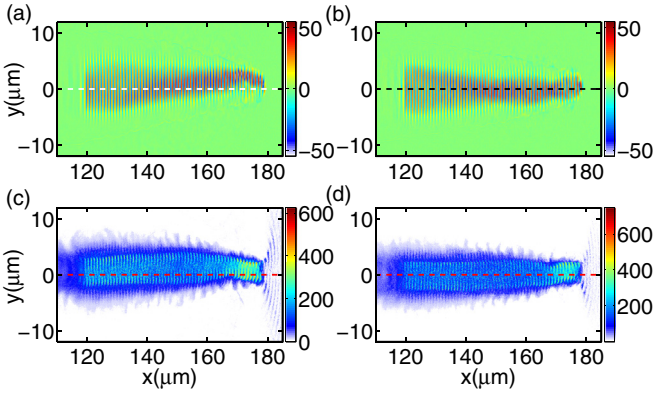

FIG. 3. The simulation results for $a_0 = 60$ and $n_0 = 1.8n_c$ in a parabolic plasma channel with $\alpha = 0.2$ [(a) and (c)] and $\alpha = 4.0$ [(b) and (d)]. (a) and (b) The distribution of the normalized transverse laser field ($eE_y/m_e\omega_0 c$) at $T = 220T_L$. (c) and (d) The distribution of the averaged electron energy (E_e) on the grids. The electron energy is in units of megaelectron volts.

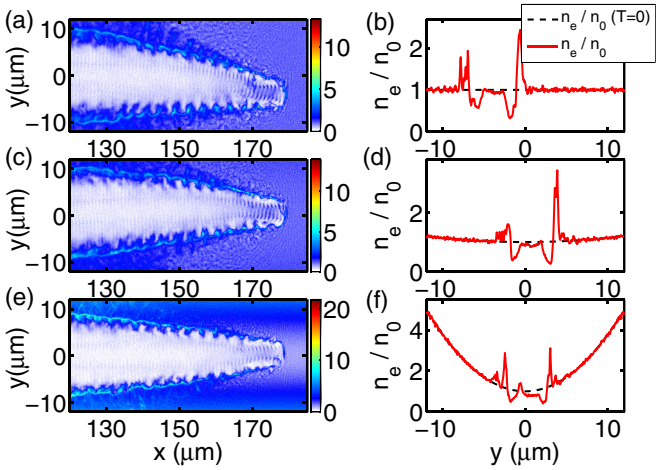

FIG. 4. [(a), (c), and (e)] The distribution of normalized electron density (n_e/n_0) at $T = 220T_L$ for different cases. [(b), (d), and (f)] The corresponding transverse density profiles [$n_e(y)/n_0$] at the laser wave front position $x = 175$ μm where the black dashed lines correspond to initial density profiles. (a) and (b) The simulation results for $\alpha = 0$; (c) and (d) the simulation results for $\alpha = 0.2$; (e) and (f) the simulation results for $\alpha = 4$.

can be produced. However, for a longer time propagation behavior, the laser hosing instability grows up as shown in Figs. 2(b) and 2(c). The laser wave front, and so as to the strong magnetic field generated in the plasma channel, gradually becomes tilted as shown in Fig. 2(f). The induced asymmetric magnetic field also makes the electron beam bend along the laser propagation direction as shown in Fig. 2(i). As a result, an off-axis and mistargeted electron beam is generated by the laser hosing process. In addition, as the asymmetric perturbation is uncontrollable, the bending direction of the electron beam would exhibit random behavior in each simulation run or experimental shot.

Figure 3 shows that by employing a preformed plasma channel the laser beam can stably propagate in the plasmas for a rather long time. For a relatively steep plasma channel with $\alpha = 4$, the restoring force provided by the parabolic plasma channel would correct the perturbed laser wave front and thus reduce the laser hosing instability. Correspondingly, the accelerated electron beams also are directed along the channel axis as shown in Fig. 3(d). Figure 4 shows the plasma density distributions for different cases. It is shown that the laser ponderomotive force expels the electrons from the laser region to form a plasma channel. The density perturbations provided by the laser ponderomotive force, as indicated by Eq. (4), would induce the hosing instability. In turn, the tilted laser pulse leads to strong tilting of the channel direction as shown in Figs. 4(a) and 4(b). While in the preformed plasma channels, the density perturbations induced by the laser ponderomotive force still exist as shown in Figs. 4(d) and 4(f), but when the density profile is steep enough, the initial density profile provides a strong restoring force, and the laser tilting behavior is suppressed. In this case, a stable density channel along the central axis is formed as shown in Fig. 4(e), and the density modulations are almost symmetrically distributed along the channel axis, which is in contrast to the case without the preformed plasma channel as shown in Figs. 4(b) and 4(f).

In order to describe the hosing instability quantitatively, one can calculate the centroid of the laser beam Y_c. If the laser beam is distributed symmetrically, then Y_c is strictly equal to zero. Once the laser beam is tilted, its centroid would deviate from zero. This parameter can well describe the degree of deviation and the growth of hosing instability. Figure 5(a) shows that, in an uniformly distributed plasma, the centroid of the laser beam increases rapidly with time. This indicates the rapid development of hosing instability. Whereas in a parabolic plasma channel, the deviation of the laser centroid is much decreased. Particularly, for a relatively steep plasma channel, a strong restoring force is provided, and the laser hosing instability can be suppressed. In this case, the centroid of the laser pulse almost remains as zero as shown in Fig. 5(a). Figure 5(b) shows the maximum absolute value of the centroid of the laser pulse for different values of α. It is demonstrated that, in an antiplasma channel with $\alpha < 0$, the laser hosing instability is further intensified, which is consistent with our theoretical predications. Whereas in a plasma channel with $\alpha > 0$, the laser hosing instability is much reduced. The value

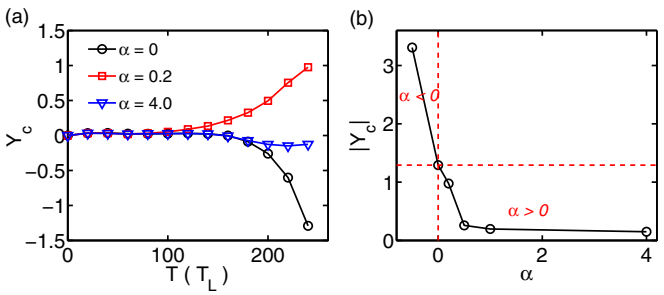

FIG. 5. (a) The time evolution of the centroid of the laser pulse in different plasma channels. (b) The maximum absolute value of the centroid of the laser pulse for different values of α. The laser and plasma parameters are the same as that in Figs. 2 and 3. The unit of Y_c is micrometers.

of the laser centroid is decreased as the value of α is increased. When the value of α is large enough ($\alpha \geqslant 0.5$) or the plasma channel is sufficiently steep, the laser hosing instability can be suppressed. In this case, the laser beam can propagate stably in the plasmas for a rather long time. Then the electrons are well guided by the channel field and adequately accelerated by the laser field as shown in Fig. 3(d) in which the maximum averaged electron energy ($\sim$750 MeV) is larger than that ($\sim$620 MeV) in Fig. 2(i).

B. Electron dynamics and radiation properties in different plasma channels

When the laser hosing instability occurs, one immediate effect is the generation of the off-axis electron beam and radiation source. In addition, this kind of instability has the characteristic of randomness, which implies that the off-axis behavior cannot be predictable. In a preformed plasma channel, the laser hosing instability is much mitigated and even suppressed. This approach would improve significantly the beam qualities of electrons and emitted photons. Figure 6 shows the angularly resolved energy distribution of the accelerated electrons and emitted photons in different cases. As a comparison, the case with $\alpha = 0$ and $n_0 = 4.2n_c$ is also considered, which corresponds to the averaged plasma density in the case of $\alpha = 4$. The averaged plasma density for a plasma channel with $\alpha > 0$ can be expressed as $\langle n_e \rangle \equiv \int_{-L}^{L} n_0(1 + \alpha y^2/L^2)dy/2L = (1 + \alpha/3)n_0$. Thus for the case with $\alpha = 4$ and $n_0 = 1.8n_c$, its averaged plasma density corresponds to $\langle n_e \rangle = (1 + 4/3)n_0 = 4.2n_c$. It is shown from Fig. 6 that, in the cases with uniform plasma density profiles, the off-axis electron beam and radiation source with a relatively large divergence angle are generated, which is induced by the severe evolution of laser hosing process. In contrast, by employing a preformed plasma channel with a steep profile, the accelerated electrons and emitted photons are well directed along the central axis. Moreover, in this case the total electron and radiation energies are concentrated within a smaller divergence angle compared with the cases without the preformed plasma channel.

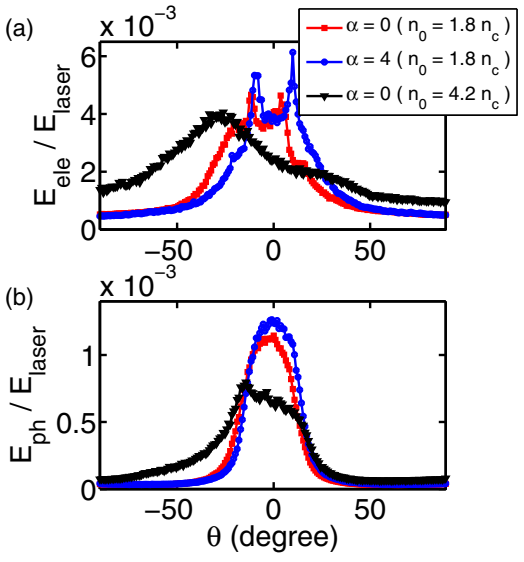

FIG. 6. Angularly resolved energy distribution of (a) the accelerated electrons and (b) the emitted photons in different plasma channels. Here θ is defined as $\theta = \arctan(p_y/p_x)$, and only the forward-going electrons and photons with $p_x > 0$ are calculated. In these simulations, the laser parameters are kept unchanged, which are the same as that in Figs. 2 and 3. The total energy of electrons and photons is normalized by the input laser energy, which is kept as constant.

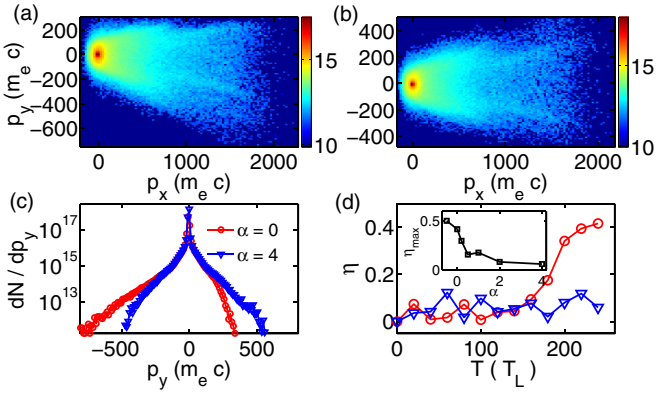

FIG. 7. The electron distribution on its momentum phase space (p_y, p_x) for (a) $\alpha = 0$ and (b) $\alpha = 4$. (c) Comparison of the electron distribution on its transverse momentum space (p_y) for different plasma channels. (d) The time evolution of the value of η in different plasma channels where the inset figure shows the maximum value of η for different values of α. In the simulations, the initial parameters are set as $a_0 = 60$ and $n_0 = 1.8n_c$, which are the same as that in Figs. 2 and 3.

On the other hand, it is noted from Fig. 7(a) that the laser hosing process results in the asymmetric distribution of electrons on the momentum phase space. This also is induced by the hosing process of the laser pulse, which exhibits a drifting velocity in a certain transverse direction. In the case with a preformed plasma channel, the electrons are distributed symmetrically on the momentum phase space as shown in Figs. 7(b) and 7(c). Based on this property, one also can define a normalized parameter, i.e., $\eta \equiv |\frac{p_+ + p_-}{p_+ - p_-}|$, to describe the laser hosing instability. Here p_+ refers to the maximum electron transverse momentum, and p_- refers to the minimum electron transverse momentum. When the electrons are distributed symmetrically on the transverse momentum space, then $p_+ + p_- = 0$ and $\eta = 0$. However, when the electrons are distributed asymmetrically, then the value of η would deviate from zero. Thus η can well describe the asymmetric degree of the electron transverse momentum space. In another way, this parameter also can reveal the growth of laser hosing instability. Figure 7(d) shows that, when the laser hosing instability occurs, the value of η increases rapidly with time. In the case with a preformed plasma channel, η oscillates around zero, suggesting that the laser hosing instability is suppressed. In addition, it is noted from the inset figure that the correlation of η with α displays a similar trend with Y_c as shown in Fig. 5(b). Thus from the viewpoint of electron properties, one also can employ the parameter η to describe the laser hosing instability.

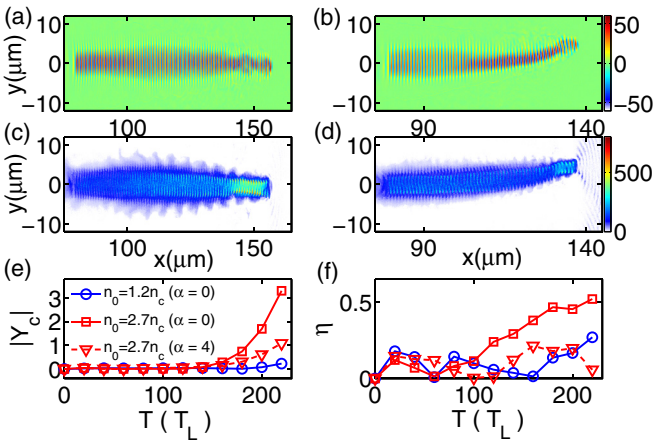

FIG. 8. The simulation results for different values of n_0/a_0n_c with a fixed laser amplitude of $a_0 = 60$ but with different plasma densities. (a) and (b) The distribution of the normalized transverse laser field ($eE_y/m_e\omega_0 c$) at $T = 180T_L$. (c) and (d) The corresponding distribution of the averaged electron energy (E_e) on the grids. (a) and (c) The simulation result for $\alpha = 0$ and $n_0/n_c = 1.2$. (b) and (d) The simulation result for $\alpha = 0$ and $n_0/n_c = 2.7$. (e) The time evolution of the centroid of the laser pulse in different cases. (f) The time evolution of the value of η in different cases.

C. The parameter study on laser hosing instability and electron dynamics

In this section, the parameter dependence of the laser hosing instability is discussed. In Sec. II, it is indicated that the hosing instability for an ultraintense laser pulse in plasmas is determined only by the parameter of n_e/a_0n_c. From Eq. (3) one can infer that with the increase in the parameter n_e/a_0n_c, the laser hosing process would be much easier to grow up. In order to check this characteristic, the parameter n_e/a_0n_c is changed by adjusting the laser intensity and the plasma density. Figure 8 shows the simulation result for a fixed laser intensity but different plasma densities. It is shown that the laser hosing process becomes more severe for a larger plasma density and is eased for a lower plasma density, compared with the result in Fig. 2. When the initial plasma density is increased, the deviation of the accelerated electron beam also becomes more severe as shown in Fig. 8(d). In addition, the asymmetric degree of the electrons also becomes larger as indicated in Fig. 8(f). Whereas even in this case, the hosing process can still be much mitigated by employing a plasma channel as shown in Figs. 8(e) and 8(f).

Figure 9 shows the laser hosing process for a fixed plasma density but with different laser intensities. It can be seen that, when the laser intensity is increased, the deviation of the laser centroid is decreased. The relativistic effect will increase the critical plasma density and thus reduce the effect of density perturbations on the laser hosing instability. In this case, the growth rate of the laser hosing process can be much decreased by improving the laser intensity as indicated by Fig. 9(d). Meanwhile, the laser group velocity also is increased as the laser intensity is increased. Thus the laser pulse with a stronger intensity also can propagate into the plasma for a longer distance as indicated by Fig. 9(c). In addition, it is noted that the laser hosing process shown in Fig. 9(b) is similar

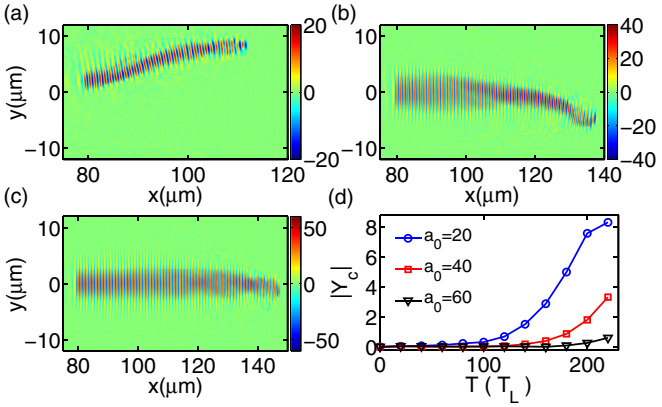

FIG. 9. The simulation results for different values of n_0/a_0n_c with a fixed plasma density $n_0 = 1.8n_c$ but with different laser intensities. (a)–(c) The distribution of the normalized transverse laser field ($eE_y/m_e\omega_0 c$) at $T = 180T_L$. (d) The time evolution of the centroid of the laser pulse in different cases. (a) The simulation result for $\alpha = 0$ and $a_0 = 20$. (b) The simulation result for $\alpha = 0$ and $a_0 = 40$. (c) The simulation result for $\alpha = 0$ and $a_0 = 60$.

to that shown in Fig. 8(b) where these two cases correspond to the same value of $n_0/a_0n_c = 0.045$ but with different laser intensities and plasma densities. In this case, the deviation of the laser centroid is almost of the same value of $|Y_c| \approx 3.5$ μm. Whereas in these two cases, the tilting direction is opposite. This also suggests the characteristic of randomness of the laser hosing process. Despite the random tilting direction, one can conclude that the hosing process of ultraintense laser pulses in plasmas is determined by the parameter n_0/a_0n_c and the growth rate increases with the value of n_0/a_0n_c.

Figure 10 shows the electron energy and momentum distributions for different laser intensities and plasma densities. It is shown from Fig. 10(a) that, for a fixed laser intensity, the maximum electron energy is decreased as the plasma density is increased. In the DLA regime, the electron acceleration length is decreased when the plasma density is increased [22].

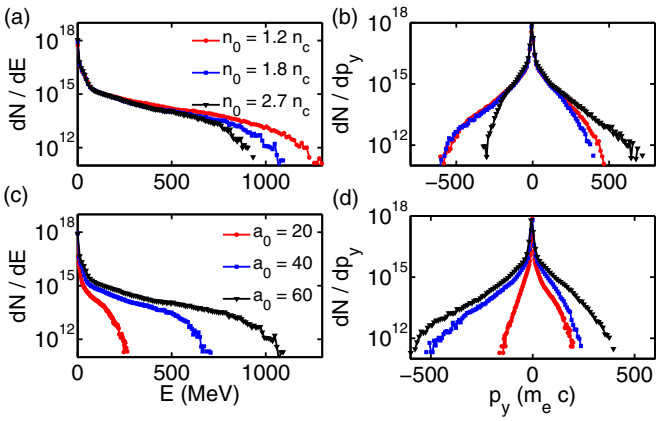

FIG. 10. The electron energy spectra [(a) and (c)] and the electron distribution on the transverse momentum space [(b) and (d)] at $T = 180T_L$ for different laser intensities and plasma densities. (a) and (b) The simulation results for a fixed laser amplitude of $a_0 = 60$ but with different plasma densities. (c) and (d) The simulation results for a fixed plasma density $n_0 = 1.8n_c$ but with different laser intensities.

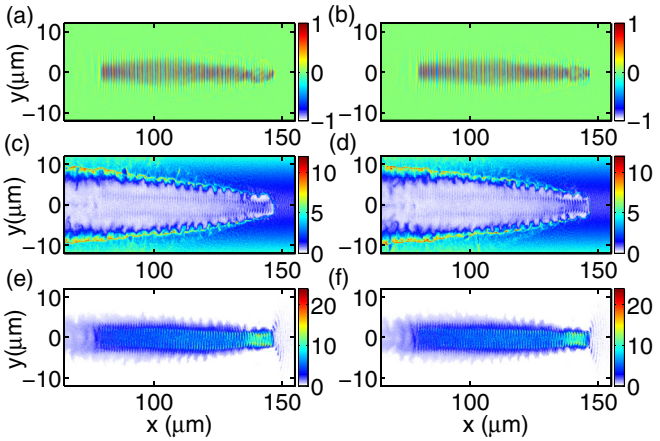

FIG. 11. The simulation results at $T = 180T_L$ for a fixed value of $n_0/a_0n_c = 0.03$ and $\alpha = 4$ but with different laser intensities. (a) and (b) The distribution of the normalized transverse laser field ($eE_y/a_0m_e\omega_0c$). (c) and (d) The normalized density (n_e/n_0) distribution of the electrons. (e) and (f) The corresponding normalized energy ($E_e/a_0m_ec^2$) distribution of the electrons. (a), (c), and (e) The simulation result for $a_0 = 40$ and $n_0 = 1.2n_c$. (b), (d), and (f) The simulation result for $a_0 = 50$ and $n_0 = 1.5n_c$.

Meanwhile, the laser hosing process also becomes more severe for a larger plasma density, which leads to asymmetrically distributed electrons on the transverse momentum space as shown in Fig. 10(b). For a fixed plasma density, it is shown from Fig. 10(c) that the maximum electron energy increases with the laser intensity. The electron momentum distribution gradually becomes symmetrical as the laser intensity is increased, suggesting that the laser hosing instability is reduced as indicated in Fig. 10(d). In addition, it is noted that the electron temperature is sensitively dependent on the laser intensity compared with the plasma density as shown in Figs. 10(a) and 10(c). When the laser intensity is increased, the temperatures of both the background electrons and the hot electrons are increased, which is strongly indicative of DLA. In this case, the plasmas become relativistically hot. The relativistic electron temperatures may reduce the hosing growth rates in a weak relativistic regime [48]. However, in the ultrarelativistic regime considered here, the thermal effect is negligible. The ratio of the thermal pressure ($P_{\rm th}$) over the laser radiation pressure ($P_{\rm rad}$) can be written as $P_{\rm th}/P_{\rm rad} = n_0T_e/a_0^2n_cm_ec^2$, which is inversely proportional to the laser intensity. Here T_e refers to the temperature of the background electrons. For the ultraintense laser pulse with $a_0 \gg 1$, the thermal pressure can be neglected compared with the laser radiation pressure. Thus, the thermal effect in our case does not affect the laser hosing process significantly.

Figure 11 shows the simulation result for fixed values of $n_0/a_0n_c = 0.03$ and $\alpha = 4$. It is shown that, in different plasma channels but with the same steepness, the normalized electric field distribution, the normalized plasma density distribution, and the normalized electron energy distribution make no difference in different cases. This indicates that the laser propagation behavior and the electron dynamics are self-similar for fixed values of n_0/a_0 and α, which agrees well with the theoretical predications in Sec. II. Once the parameter n_0/a_0 is fixed, the phase velocity of the laser pulse, the electron beam radius, and the electron acceleration time are all determined [22]. When the steepness of the plasma channel or the value of α also is fixed, the growth of the laser hosing instability would become the same in different plasma channels, except for the tilting direction of the laser pulse.

IV. CONCLUSION

In conclusion, the laser hosing process in different plasma channels is investigated in the DLA regime. The corresponding electron dynamics and radiation properties also are discussed. It is proposed that the laser hosing instability can be mitigated and even suppressed by using a relatively steep parabolic plasma channel. In the case without a preformed plasma channel, the laser hosing process would grow up rapidly and lead to the generation of randomly tilted electron beams and radiation sources. Whereas in the case with a preformed plasma channel, electrons can be well guided, and the emitted photons are well directed along the channel axis. In addition, compared with the case without a preformed plasma channel, the electrons and photons are concentrated within a much smaller divergence angle. The employment of a preformed plasma density channel can stably guide the relativistically intense laser pulse and thus can greatly improve the properties of the electron beam and radiation source that are produced especially in the DLA regime. In the experiments, the plasma density channel can be produced by the ponderomotive expulsion of plasmas from another guiding laser pulse [49] or using slow capillary discharge [50] and the igniter-heater technique [51].

ACKNOWLEDGMENTS

This work was supported by the National Key Programme for S&T Research and Development Grant No. 2016YFA0401100, the National Natural Science Foundation of China (NSFC) Grants No. 91230205 and No. 11575031, the National Basic Research 973 Project No. 2013CB834100, and the NSAF, Grant No. U1630246. The computational resources were supported by the Special Program for Applied Research on Super Computation of the NSFC-Guangdong Joint Fund (the second phase). The EPOCH code was developed under the U.K. EPSRC Grants No. EP/G054940/1, No. EP/G055165/1, and No. EP/G056803/1. B.Q. acknowledges support from the Thousand Young Talents Program of China. T.W.H would like to thank K. D. Xiao, S. L. Yang, L. B. Ju, H. X. Chang, Y. X. Zhang, W. P. Yao, and Z. Xu at Peking University for their help and useful discussions on this paper.

[1] S. Corde *et al.*, Rev. Mod. Phys. **85**, 1 (2013).
[2] S. P. D. Mangles *et al.*, Nature (London) **431**, 535 (2004).
[3] C. G. R. Geddes *et al.*, Nature (London) **431**, 538 (2004).
[4] J. Faure *et al.*, Nature (London) **431**, 541 (2004).

[5] W. P. Leemans *et al.*, Nat. Phys. **2**, 696 (2006).
[6] X. Wang *et al.*, Nat. Commun. **4**, 1988 (2013).
[7] H. T. Kim, K. H. Pae, H. J. Cha, I. J. Kim, T. J. Yu, J. H. Sung, S. K. Lee, T. M. Jeong, and J. Lee, Phys. Rev. Lett. **111**, 165002 (2013).
[8] W. P. Leemans *et al.*, Phys. Rev. Lett. **113**, 245002 (2014).
[9] E. Esarey, B. A. Shadwick, P. Catravas, and W. P. Leemans, Phys. Rev. E **65**, 056505 (2002).
[10] S. Kiselev, A. Pukhov, and I. Kostyukov, Phys. Rev. Lett. **93**, 135004 (2004).
[11] S. Kneip *et al.*, Nat. Phys. **6**, 980 (2010).
[12] S. Cipiccia *et al.*, Nat. Phys. **7**, 867 (2011).
[13] T. Tajima and J. M. Dawson, Phys. Rev. Lett. **43**, 267 (1979).
[14] A. Pukhov, Z. M. Sheng, and J. Meyer-ter-Vehn, Phys. Plasmas **6**, 2847 (1999).
[15] W. Lu, M. Tzoufras, C. Joshi, F. S. Tsung, W. B. Mori, J. Vieira, R. A. Fonseca, and L. O. Silva, Phys. Rev. Spec. Top.-Accel. Beams **10**, 061301 (2007).
[16] C. Gahn, G. D. Tsakiris, A. Pukhov, J. Meyer-ter-Vehn, G. Pretzler, P. Thirolf, D. Habs, and K. J. Witte, Phys. Rev. Lett. **83**, 4772 (1999).
[17] S. P. D. Mangles *et al.*, Phys. Rev. Lett. **94**, 245001 (2005).
[18] B. Qiao *et al.*, Phys. Plasmas **12**, 083102 (2005); H. Y. Niu *et al.*, Laser Part. Beams **26**, 51 (2008).
[19] B. Liu, H. Y. Wang, J. Liu, L. B. Fu, Y. J. Xu, X. Q. Yan, and X. T. He, Phys. Rev. Lett. **110**, 045002 (2013).
[20] R. H. Hu *et al.*, Sci. Rep. **5**, 15499 (2015).
[21] B. Liu *et al.*, Phys. Plasmas **22**, 080704 (2015).
[22] T. W. Huang, A. P. L. Robinson, C. T. Zhou, B. Qiao, B. Liu, S. C. Ruan, X. T. He, and P. A. Norreys, Phys. Rev. E **93**, 063203 (2016).
[23] G. Z. Sun *et al.*, Phys. Fluids **30**, 526 (1987).
[24] A. B. Borisov *et al.*, Plasma Phys. Controlled Fusion **37**, 569 (1995).
[25] A. Pukhov and J. Meyer-ter-Vehn, Phys. Rev. Lett. **76**, 3975 (1996).
[26] K. A. Tanaka *et al.*, Phys. Rev. E **62**, 2672 (2000).
[27] H. Y. Wang *et al.*, Phys. Rev. Lett. **107**, 265002 (2011).
[28] C. Ren and W. B. Mori, Phys. Plasmas **8**, 3118 (2001).
[29] G. Shvets and J. S. Wurtele, Phys. Rev. Lett. **73**, 3540 (1994).
[30] P. Sprangle, J. Krall, and E. Esarey, Phys. Rev. Lett. **73**, 3544 (1994).
[31] B. J. Duda and W. B. Mori, Phys. Rev. E **61**, 1925 (2000).
[32] L. Ceurvorst *et al.*, New J. Phys. **18**, 053023 (2016).
[33] G. Li, R. Yan, C. Ren, T.-L. Wang, J. Tonge, and W. B. Mori, Phys. Rev. Lett. **100**, 125002 (2008).
[34] L. Willingale *et al.*, Phys. Rev. Lett. **106**, 105002 (2011); New J. Phys. **15**, 025023 (2013).
[35] T. W. Huang, C. T. Zhou, A. P. L. Robinson, B. Qiao, H. Zhang, S. Z. Wu, H. B. Zhuo, P. A. Norreys, and X. T. He, Phys. Rev. E **92**, 053106 (2015).
[36] L. B. Ju *et al.*, Phys. Rev. E **94**, 033202 (2016).
[37] T. W. Huang, C. T. Zhou, and X. T. He, Laser Part. Beams **33**, 347 (2015).
[38] C. T. Zhou, X. T. He, and L. Y. Chew, Opt. Lett. **36**, 924 (2011).
[39] C. T. Zhou, L. Y. Chew, and X. T. He, Appl. Phys. Lett. **97**, 051502 (2010).
[40] T. Kluge *et al.*, New J. Phys. **14**, 023038 (2012).
[41] K. D. Xiao *et al.*, AIP Adv. **6**, 015303 (2016).
[42] X. L. Zhu *et al.*, New J. Phys. **17**, 053039 (2015).
[43] D. J. Stark, T. Toncian, and A. V. Arefiev, Phys. Rev. Lett. **116**, 185003 (2016).
[44] T. W. Huang *et al.*, Appl. Phys. Lett. **110**, 021102 (2017).
[45] C. D. Decker and W. B. Mori, Phys. Rev. Lett. **72**, 490 (1994).
[46] S. Gordienko and A. Pukhov, Phys. Plasmas **12**, 043109 (2005).
[47] T. D. Arber *et al.*, Plasma Phys. Controlled Fusion **57**, 113001 (2015).
[48] G. Li, W. B. Mori, and C. Ren, Phys. Rev. Lett. **110**, 155002 (2013).
[49] K. Krushelnick, A. Ting, C. I. Moore, H. R. Burris, E. Esarey, P. Sprangle, and M. Baine, Phys. Rev. Lett. **78**, 4047 (1997).
[50] Y. Ehrlich, C. Cohen, A. Zigler, J. Krall, P. Sprangle, and E. Esarey, Phys. Rev. Lett. **77**, 4186 (1996).
[51] P. Volfbeyn, E. Esarey, and W. P. Leemans, Phys. Plasmas **6**, 2269 (1999).